Revealing the Incidence-Angle-Independent Frequency Shift in the Acoustic Rotational Doppler Effect

Chuanxin Zhang,[1] Xue Jiang,[1,2,*] and Dean Ta[1,2,†]
[1]Center for Biomedical Engineering, School of Information Science and Technology, Fudan University, Shanghai 200433, China
[2]State Key Laboratory of Integrated Chips and System, Fudan University, Shanghai 200433, China

(Received 29 August 2023; accepted 21 February 2024; published 13 March 2024; corrected 15 March 2024)

The Doppler effect is a universal wave phenomenon that has inspired various applications due to the induced frequency shift. In the case of the linear Doppler effect, the frequency shift depends on the incident frequency and angle. Here, we unveil the frequency shift dependence induced by the acoustic rotational Doppler effect in the wave-object scattering process. We experimentally demonstrate that this frequency shift is exclusively determined by the angular speed and rotational symmetry of the spinning scatterer while remaining independent of the incident angular momentum and angle. We derive the analytical relationship between the frequency shift and the scatterer's helicity, presenting a novel approach for helical feature recognition. The angle-independent nature of the frequency shift inherently prevents spectrum broadening and offers a solution for precise motion measurement through the rotational Doppler effect. This work provides a rigorous and comprehensive understanding of the acoustic Doppler effect, enriching its applications in helicity and motion detection.

DOI: 10.1103/PhysRevLett.132.114001

Introduction.—The Doppler effect is a universal wave phenomenon and one of the fundamental mechanisms in physics. It is responsible for the shift in wave frequency, reflecting the relative motion and characteristics of the moving scatterer interacting with the wave [1]. First proposed by Doppler in 1842 and later tested in sound waves by Ballot in 1845 [2], the Doppler effect has been recognized to exist in virtually any wave system and has inspired diverse applications, including Doppler ultrasonography, radar remote sensing, laser vibrometry, and astrosurveillance [3–8].

In acoustics, the most widely known Doppler effect is the linear Doppler effect (LDE), which originates from linear momentum. When interacting with an object of translational velocity v, the reflected sound will acquire a diploid frequency shift of $\Delta f_{\mathrm{LDE}} = 2v\cos\theta/\lambda_0$, where v represents the relative motion velocity, λ_0 is the wavelength of the incident wave, and θ is the incident angle [3], as illustrated in Fig. 1(a). This illustration demonstrates that the Doppler shift depends on the incident angle. This dependence on incident angle leads to the limited accuracy in Doppler metrology due to the practical uncertainty in incident angle [9].

In addition to linear momentum, angular momentum contributes to the Doppler shift [4,10–14]. The relative rotation between the source and observer gives rise to the rotational Doppler effect (RDE), offering a strategy for precise rotation measurement, mimicking superradiance acoustically, and exploring nonreciprocity in the laboratory [15–18]. An example of RDE involves detecting a vortex beam carrying orbital angular momentum (OAM) [19] with a rotating sensor. The detected wave acquires a frequency shift of $\Delta f_{\mathrm{RDE}} = l_{\mathrm{in}}\Omega/2\pi$ [20], with l_{in} representing the OAM order of the incident vortex and Ω representing the rotational angular velocity. Additionally, RDE occurs in the wave-object scattering process. When a nonrotating sound wave interacts with a spinning rough plate, it has been demonstrated that the frequency shift of the normally scattered sound is also expressed as $\Delta f_{\mathrm{RDE}} = l_{\mathrm{in}}\Omega/2\pi$ [4]. From these conventional illustrations of LDE and RDE in acoustics, it seems that the Doppler shift should always depend on the incident wave. In optics, it has been reported that the spiral phase distribution of the spinning object affects the RDE frequency content in transmitted light [4,21,22]. Nevertheless, the analysis method based on geometrical optics cannot be directly applied to wave acoustics. Despite its significance in physics and a variety of applications, a definitive conclusion and comprehensive physical interpretation of the Doppler shift in acoustic RDE have been lacking.

This Letter presents evidence for the incidence-angle-independent nature of the Doppler shift in acoustic RDE. The Doppler shift in the sound-scatterer interaction process is independent of the incident OAM order and incident angle. Through a theoretical analysis of the spatial-temporal evolution of OAM and a complete decomposition of the scattering modes, we demonstrate that it is the rotational symmetry order M of the spinning scatterer, rather than the l_{in} of the incident sound, that determines the Doppler shift [Fig. 1(b)]. Moreover, in contrast to the θ dependence observed in LDE, the frequency shift in RDE is irrelevant to the incident angle [Fig. 1(c)]. We experimentally verified

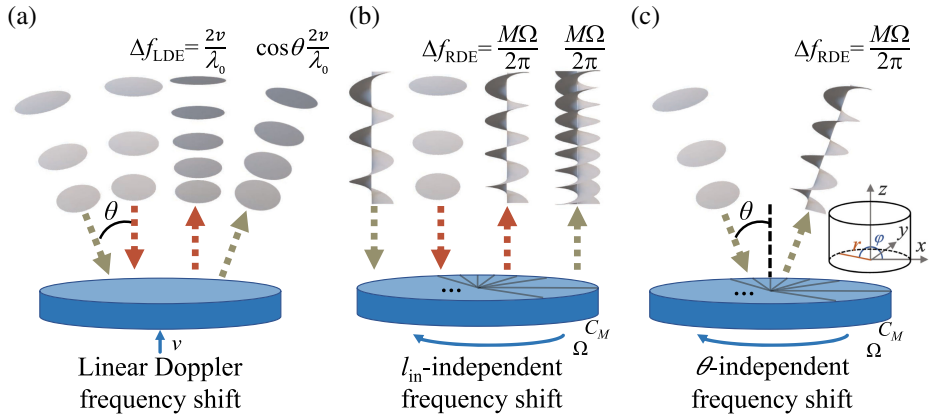

FIG. 1. Comparison of the frequency shift induced by linear and rotational Doppler effect in acoustics. (a) The linear Doppler frequency shift Δf_{LDE} of the sound wave reflected from a moving plate depends on the incident wavelength λ_0 and incident angle θ, and is given by $\Delta f_{\mathrm{LDE}} = 2v\cos\theta/\lambda_0$. (b),(c) Sound wave reflected from the helical phase plate of C_M symmetry (i.e., the plate repeats upon rotation by $2\pi/M$) and Ω rotational angular velocity acquires the frequency shift $\Delta f_{\mathrm{RDE}} = M\Omega/2\pi$, independent on both the incident OAM order l_{in} and the incident angle θ.

these independencies by directing an ultrasound vortex onto a spinning helical phase metasurface with C_M symmetry, where C_M represents rotational symmetry of order M. We observed that Δf_{RDE} varied with M but remained constant regardless of different incident OAM orders l_{in} and incident angles θ. This distinctive characteristic of incident-independent Δf_{RDE} holds promise for precise rotation detection without needing correction to compensate for spectrum broadening caused by varying incident angles. Our study advances the understanding of the acoustic Doppler effect and highlights its potential for applications in remote measurements and object feature recognition.

Result.—Models and theory: We theoretically derive the incidence-angle-independent Δf_{RDE} using the multiple scattering mode decomposition method in OAM space. To maintain generality, we consider a plate positioned in the r-φ plane ($z = 0$) and rotating around the z axis. Thanks to the orthogonality of different OAM modes $e^{jl\varphi}$, they can serve as a set of orthogonal bases to decompose any field $f(r,\varphi)$ into its constituent OAM modes. This decomposition is achieved through a Fourier transform applied to the azimuthal angle φ in the polar coordinate system, represented mathematically as [23]

$$\frac{1}{2\pi}\int_{-\pi}^{\pi} e^{jl'\varphi}e^{jl\varphi}\mathrm{d}\varphi = \begin{cases} 1, & l = l' \\ 0, & l \neq l' \end{cases}. \tag{1}$$

$$F(r,l) = \frac{1}{2\pi}\int_{-\pi}^{\pi} f(r,\varphi)e^{-jl\varphi}\mathrm{d}\varphi. \tag{2}$$

In this context, $F(r,l)$ represents the intensity component associated with the OAM mode $e^{jl\varphi}$ at radius r. Consequently, the incident sound field interacting with the rotating plate at the incident angle θ can be expressed in the OAM space as

$$p_{\mathrm{in}}(r,\varphi,t;\theta) = \sum_{l_{\mathrm{in}}} \mathrm{A}_{l_{\mathrm{in}}}(r;\theta)e^{j(\omega_0 t + l_{\mathrm{in}}\varphi)}, \tag{3}$$

where ω_0 represents the angular frequency of the incident sound, and $A_{l_{\mathrm{in}}}$ represents the expansion coefficient that denotes the corresponding amplitude distribution for the l_{in} OAM component. The incident angle θ essentially adjusts the OAM's reference direction, which is equivalent to introducing a tilted phase, affecting the amplitude component $A_{l_{\mathrm{in}}}$. Similarly, the scattering properties of the rotating plate can also be expressed in terms of its scattering coefficient in the OAM space as

$$S(r,\varphi,t) = \sum_{M} B_M(r)e^{j[M(\varphi+\Omega t)]}, \tag{4}$$

where $B_M(r)$ represents the component in the M th OAM mode, and $\varphi + \Omega t$ is resulted from the rotation at an angular velocity Ω.

It is worth noting that the phase rotation pattern and OAM carried by the scattered beam reverse their direction in reference to the propagation direction, resulting in an opposite OAM order $(-l_{\mathrm{in}})$ [24]. Consequently, upon the interaction with the rotating plate, the scattered wave can be expressed as

$$\begin{aligned} p_{\mathrm{s}}(r,\varphi,t;\theta) &= p_{\mathrm{in}}S = \sum_{M} p_M \\ &= \sum_{M}\sum_{l_{\mathrm{in}}} A_{l_{\mathrm{in}}}(r;\theta)B_M(r)e^{j[(\omega_0+M\Omega)t+(M-l_{\mathrm{in}})\varphi]}. \end{aligned} \tag{5}$$

We extract p_M as the scattered wave generated with the M th order OAM component of the rotating plate. The phase front $e^{j(M-l_{\mathrm{in}})\varphi}$ in Eq. (5) indicates that the OAM

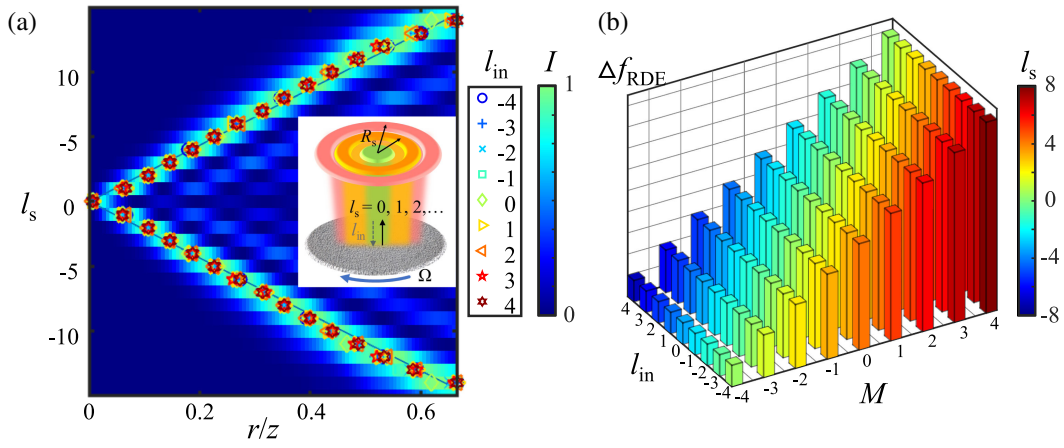

FIG. 2. Dependences of scattered OAM spectrum and Doppler shift on incident OAM order l_{in} and OAM order M of the scatterer. (a) OAM spectrum of the wave scattered by a uniformly rough plate [i.e., the plate possesses the even-distributed OAM components in Eq. (4)] calculated from numerical simulation, as functions of the scattered OAM order l_s and radial position r. Here, the incident OAM order $l_{in} = 0$ and incident angle $\theta = 0$. The radial position R_s of the brightest spectrum for each l_s value indicates the corresponding intensity peak (illustrated in the inset). As a comparison, intensity peaks R_s for different l_{in} values ($\theta = 0$) are denoted by different markers. The OAM spectrum is determined by l_s and is consistent for different l_{in}. (b) Relationships among l_{in}, l_s, M, and Δf_{RDE} obtained from simulations. The axes represent l_{in} and M, the color of the bars corresponds to l_s, and the height of the bars represents Δf_{RDE}. These results confirm the extracted relationship $l_s = M - l_{in}$, aligning with the theoretical predictions. The rotational Doppler shift is exclusively determined by the OAM order M of the scatterer.

order of the scattered wave is $l_s = M - l_{in}$. The angular frequency of the p_M scattered wave is determined as

$$\omega_M = \frac{\mathrm{dArg}(p_M)}{\mathrm{d}t} = \omega_0 + M\Omega. \tag{6}$$

This theoretical model illustrates that the scattered OAM pattern results from the interaction between the incident wave and the scatterer's features, which are determined by the incident parameters (l_{in}, θ) and the scatterer's characteristics (M). The incident angle θ is mapped into the amplitude component and affects the scattered OAM patterns. Notably, the absence of l_{in} and θ in Eq. (6) explicitly demonstrates the incidence-independence nature of the rotational Doppler shift, which is solely determined by the OAM order M of the scatterer and the rotational angular velocity Ω.

The scattered sound wave propagating after the interaction is calculated using the Rayleigh-Sommerfeld diffraction integral method [25], with the sound distribution on the $z = 0$ plane serving as the boundary condition. We have developed a set of custom scripts [26,27] written in MATLAB to model the wave-scatterer interaction numerically. This method includes an effective temporal simulation to extract the rotational Doppler shift from the temporal signals [14]. This numerical simulation method enables us to investigate the relationships among l_{in}, l_s, M, and Δf_{RDE} and verify the theoretical conclusions.

As an example, we consider a rotating plate with a uniform scattering coefficient S within $M \in [-90, 90]$ as an illustration, dubbed as the uniformly rough plate. In Fig. 2(a), we illustrate the OAM spectrum of the scattered field along the radius under normal plane wave illumination $(l_{in} = 0, \theta = 0)$. Here, the radial position (R_s) of the brightest spectrum indicates the intensity peak for each l_s value. We further extract these R_s values under varying incident l_{in} and represent them with different markers in Fig. 2(a). It is evident that R_s consistently increases with $|l_s|$ regardless of l_{in}. Consequently, the Doppler shifts (Δf_{RDE}) for different scattered orders l_s can be effectively captured by detecting at the appropriate R_s. The results presented in Fig. 2(a) explain the seeming l_{in}-dependent Δf_{RDE} observed in vertically scattered waves by arbitrary rough plates. For instance, when considering a vertically incident $(\theta = 0)$ with an OAM order l_{in}, detection at $r = 0$ functions as spatial filtering to exclusively collect the 0 th order OAM component, i.e., $l_s = M - l_{in} = 0$, since the other OAM components degenerate at the center. Consequently, the detected Doppler shift is given by $\Delta f_{RDE} = M\Omega/2\pi = l_{in}\Omega/2\pi$, giving rise to the seeming l_{in}-dependent behavior observed in the conventional case of arbitrary rough plates.

As an additional illustration to succinctly demonstrate the physics behind M-determined Doppler shifts, we conducted numerical simulations to model the scattering of a pure vortex beam by a rotating helical phase metasurface with C_M symmetry. In this scenario, the scattered field contains only one OAM component. The calculated values of l_s and Δf_{RDE} from these simulations are presented in Fig. 2(b), where the axes represent l_{in} and M, the color of the bars indicates the l_s values, and the height of the bars represents the Δf_{RDE} values. These results confirm the extracted relationship $l_s = M - l_{in}$ and the l_{in}-independent

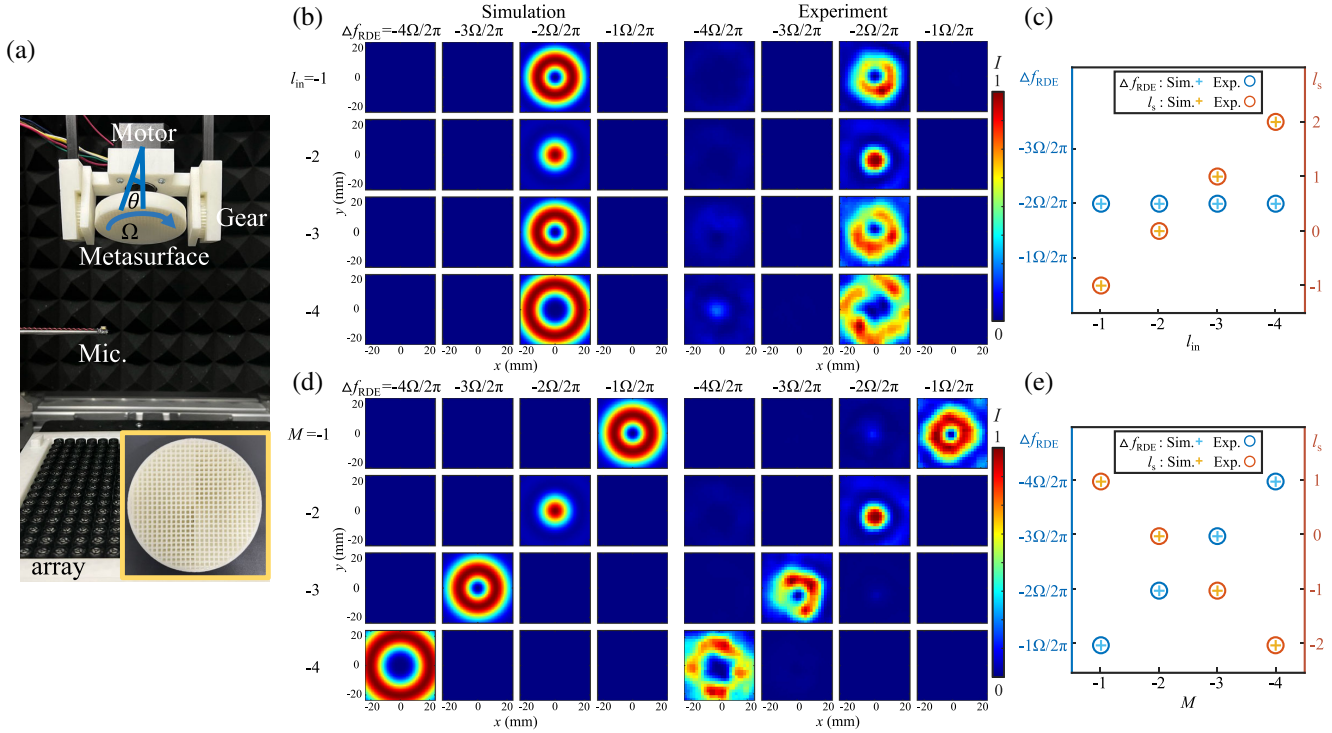

FIG. 3. Experimental verification of the l_{in}-independent rotational Doppler shift. (a) Photograph of the experimental system consisting of an emitting array, a rotating helical phase metasurface controlled by a motor, and a field-scanning microphone. Inset: photograph of a 3D-printed metasurface ($M = -2$). (b) Summary of scattered fields at different frequencies obtained from simulations and experiments, scattered by the same metasurface ($M = -2$) while illuminated with different vortex beams (l_{in} from -4 to -1). (c) The extracted Doppler shift Δf_{RDE} and scattered OAM order l_{s}, as functions of the incident OAM order l_{in}. (d) Summary of the scattered fields at different frequencies, illuminated with the same vortex beam ($l_{\mathrm{in}} = -2$) while scattered by different metasurface (M from -4 to -1). (e) Relationships among the Doppler shift Δf_{RDE}, l_{s} of the scattered wave, and M of the helical metasurface.

nature of the Doppler shift, aligning with the theoretical predictions.

Experimental observation: We experimentally investigated the incidence-angle-independent Δf_{RDE} in an airborne ultrasound system [Fig. 3(a)]. Ultrasound vortex beams at 40 kHz are generated using a 16×16 transducer array. The incident OAM order l_{in} varied from -4 to -1. Helical phase metasurfaces with different C_M symmetries were designed by assembling Fabry-Perot resonators to provide the required azimuth-dependent phase profile [28]. A photograph of the 3D-printed metasurfaces ($M = -2$) is presented in Fig. 3(a). The metasurface, located 200 mm away from the emitting array, was physically rotated by a motor with a controllable angular velocity Ω and coaxially aligned with the center of the incident vortex beam. The angular orientation of the metasurface relative to the incident beam could be precisely adjusted using gears. We performed field scanning of the scattered wave within a 40×40 mm^2 area, positioned 100 mm away from the metasurface, with a 2 mm scanning step. The scattered fields at different frequencies were reconstructed by extracting the corresponding spectral components from the Fourier transform of the measured temporal signals.

Figure 3 presents a comparison between numerical simulations and experimental results of scattered fields at different frequencies for varying incident illuminations [Fig. 3(b)] or different helical phase metasurfaces [Fig. 3(d)]. We initially analyze the dependence on the incident OAM order by controlling l_{in} from -4 to -1 while maintaining the rotational symmetry and angular velocity of the metasurface at $M = -2$ and $\Omega = 10 \times 2\pi$ rad/s. Both in simulation and experiment, it is observed that the scattered wave vanishes at frequencies other than $\Delta f_{\mathrm{RDE}} = -2\Omega/2\pi$, regardless of the incident OAM order l_{in}. Instead, the influence of l_{in} is reflected in the scattered pattern and the scattered OAM order l_{s}. The extracted relationships among Δf_{RDE}, l_{s}, and l_{in} in Fig. 3(c) demonstrate the independence between Δf_{RDE} and l_{in}. The scattered OAM order l_{s} varies with l_{in} as theoretically predicted. The slight spectrum leakage to other frequencies experimentally observed may be attributed to several factors, including imperfections in the metasurface, mechanical vibrations, and instabilities in the rotational speed.

Subsequently, we explore the relationship between Δf_{RDE} and M by emitting identical vortex beams ($l_{\mathrm{in}} = -2$) while scattering them with different metasurfaces

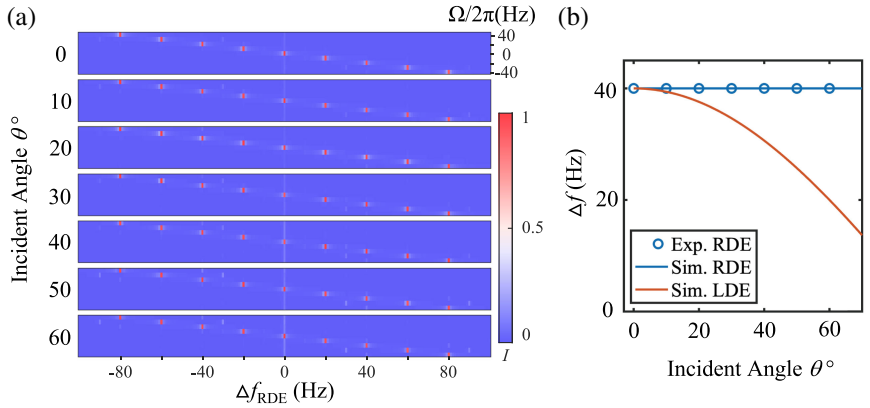

FIG. 4. Independence of rotational Doppler shift on incident angle. (a) Normalized frequency spectra of ultrasound wave scattered by the rotating helical metasurface, with different angular velocity Ω and incident angle θ. The results are measured from experiments. (b) The extracted frequency shift of rotational Doppler effect (RDE) and linear Doppler effect (LDE), as functions of incident angle θ.

(M ranging from -4 to -1) rotating at a constant Ω. In this scenario, both the Doppler shift and the scattered pattern are influenced by M: the Doppler shift follows $\Delta f_{\mathrm{RDE}} = M\Omega/2\pi$, and the scattered OAM order adheres to $l_s = M + 2$. The consistency among the theory, simulations, and experimental results provides strong evidence for the l_{in}-independent frequency shift induced by acoustic RDE.

Another crucial consequence of RDE derived from our analytical model is the θ-independent frequency shift. This behavior is fundamentally distinct from that of LDE. To experimentally confirm this, we varied the incident angle and analyzed the frequency spectrum of the scattered wave. A helical metasurface with $M = -2$, rotating at different angular (Ω ranging from $-40 \times 2\pi$ to $40 \times 2\pi$ rad/s), was illuminated by a vortex beam with identical OAM order $l_{\mathrm{in}} = -2$ but different incident angles (θ ranging from 0° to 60°). The measured frequency spectra (normalized with the respective maximum values) are plotted in Fig. 4(a). Notably, the spectral patterns remained nearly identical regardless of θ. Under all incident angles, Δf_{RDE} consistently increased linearly with Ω, as predicted by Eq. (6). A comparison of the dependence on the incident angle in LDE($2v/\lambda_0 = 40$ Hz) and RDE($M = -2, \Omega = -20$ rad/s) is shown in Fig. 4(b). Another distinct feature in Fig. 4(a) is the absence of spectrum broadening. In RDE, Δf_{RDE} only occurs at discrete values due to the integer nature of the OAM order. The influence of incident angle is primarily reflected in the scattered pattern, which affects the signal amplitude measured at a particular position. Therefore, the inherent immunity to spectrum broadening provided by the θ independence makes the rotational Doppler shift promising for precise velocimetry and rotation detection. Additionally, the frequency shift exclusively determined by M and Ω also offers a simple and clear principle for recognizing the helical features of complex objects.

Summary and outlook.—In this study, we have elucidated the incident-independent nature of rotational Doppler shift in the sound-scatterer interaction, employing a combination of theoretical modeling, numerical simulations, and experimental measurements. The rotational Doppler shift is determined by the rotational symmetry of the scatterer rather than the incident OAM order. We have also discovered a constant frequency shift independent of the incident angle θ. These theoretical conclusions have been experimentally validated by measuring the relationships among Doppler shift, incident OAM order, incident angle, and the rotational symmetry of the scatterer. Unlike the classical model used for analyzing optical RDE which assumes that the vortex beam is a linear superposition of oblique light rays at small incident angles, our scattering model based on the wave acoustics principle considers the actual characteristics of the vortex beam without relying on these assumptions.

As an example of the practical applications of incident independence, we have demonstrated the remote detection of rotational speed via ultrasound. In contrast to LDE, this approach consistently provides accurate results regardless of the detection angle. The RDE mechanism holds potential to advance sonic nondestructive testing. For instance, in aerospace, it could contribute to remote sensing for tracking and monitoring rotating objects, providing angle-independent rotational measurements. Additionally, in biomedical imaging, it could lead to more accurate and noninvasive rotational velocity detection which is critical in blood vessel diagnostics. Furthermore, the scattered OAM spectrum has been reported to assist in object feature retrieval and imaging [29,30]. Therefore, by linking the OAM spectrum with the frequency spectrum through RDE, our findings could offer a simpler, more robust approach to object imaging and feature recognition.

This work is supported by the National Natural Science Foundation of China (Grants No. T2222024 and No. 12034005), the National Key R&D Program of

China (Grants No. 2023YFA1407800 and No. 2022YFA1404500), the STCSM Science and Technology Innovation Plan of Shanghai Science and Technology Commission (Grant No. 21JC1400300).

*Corresponding author: xuejiang@fudan.edu.cn
†Corresponding author: tda@fudan.edu.cn

[1] C. H. Papas, *Theory of Electromagnetic Wave Propagation* (Courier Corporation, New York, 2014).
[2] B. Ballot, Ann. Phys. (Berlin) **142**, 321 (1845).
[3] D. L. Franklin, W. Schlegel, and R. F. Rushmer, Science **134**, 564 (1961).
[4] M. P. Lavery, F. C. Speirits, S. M. Barnett, and M. J. Padgett, Science **341**, 537 (2013).
[5] H. S. Zapolsky, Science **153**, 635 (1966).
[6] T. Asakura and N. Takai, Appl. Phys. **25**, 179 (1981).
[7] R. Meynart, Appl. Opt. **22**, 535 (1983).
[8] V. C. Chen, F. Li, S.-S. Ho, and H. Wechsler, IEEE Trans. Aerospace Electron. Syst. **42**, 2 (2006).
[9] J. A. Jensen, *Estimation of Blood Velocities Using Ultrasound: A Signal Processing Approach* (Cambridge University Press, Cambridge, England, 1996).
[10] B. A. Garetz, J. Opt. Soc. Am. **71**, 609 (1981).
[11] O. Korech, U. Steinitz, R. J. Gordon, I. S. Averbukh, and Y. Prior, Nat. Photonics **7**, 711 (2013).
[12] G. M. Gibson, E. Toninelli, S. A. Horsley, G. C. Spalding, E. Hendry, D. B. Phillips, and M. J. Padgett, Proc. Natl. Acad. Sci. U.S.A. **115**, 3800 (2018).
[13] G. Li, T. Zentgraf, and S. Zhang, Nat. Phys. **12**, 736 (2016).
[14] C. Zhang, X. Jiang, J. He, Y. Li, and D. Ta, Adv. Sci. **10**, 2206619 (2023).
[15] M. Cromb, G. M. Gibson, E. Toninelli, M. J. Padgett, E. M. Wright, and D. Faccio, Nat. Phys. **16**, 1069 (2020).
[16] D. Faccio and E. M. Wright, Phys. Rev. Lett. **123**, 044301 (2019).
[17] D. Deng, H. Zhao, J. Ni, Y. Li, and C.-W. Qiu, Nanophotonics **11**, 865 (2021).
[18] Q. Wang, Z. Zhou, D. Liu, H. Ding, M. Gu, and Y. Li, Sci. Adv. **8**, eabq4451 (2022).
[19] X. Jiang, Y. Li, B. Liang, J. C. Cheng, and L. Zhang, Phys. Rev. Lett. **117**, 034301 (2016).
[20] K. Skeldon, C. Wilson, M. Edgar, and M. Padgett, New J. Phys. **10**, 013018 (2008).
[21] J. Leach, S. Keen, M. J. Padgett, C. Saunter, and G. D. Love, Opt. Express **14**, 11919 (2006).
[22] H. Zhou, D. Fu, J. Dong, P. Zhang, and X. Zhang, Opt. Express **24**, 10050 (2016).
[23] E. Yao, S. Franke-Arnold, J. Courtial, S. Barnett, and M. Padgett, Opt. Express **14**, 9071 (2006).
[24] Z. Zou, R. Lirette, and L. Zhang, Phys. Rev. Lett. **125**, 074301 (2020).
[25] P. M. Morse and K. U. Ingard, *Theoretical Acoustics* (Princeton University Press, Princeton, NJ, 1986).
[26] C. Zhang, X. Jiang, S. Han, J. He, Y. Zheng, B. Li, and D. Ta, Appl. Phys. Rev. **9**, 041413 (2022).
[27] C. Zhang, J. He, X. Jiang, and D. Ta, Adv. Intell. Syst. **5**, 2300255 (2023).
[28] M. Yang, S. Chen, C. Fu, and P. Sheng, Mater. Horiz. **4**, 673 (2017).
[29] G. Xie *et al.*, Opt. Lett. **42**, 4482 (2017).
[30] T. Brunet, J.-L. Thomas, and R. Marchiano, Phys. Rev. Lett. **105**, 034301 (2010).

Correction: The title contained minor errors in wording and has been fixed.